Bounding quantum dark forces

Philippe Brax,[1,*] Sylvain Fichet,[2,†] and Guillaume Pignol[3,‡]
[1]Institut de Physique Théorique, Université Paris-Saclay, CEA, CNRS, F-91191 Gif/Yvette Cedex, France
[2]ICTP-SAIFR & IFT-UNESP, R. Dr. Bento Teobaldo Ferraz 271, São Paulo 01140-070, Brazil
[3]Laboratoire de Physique Subatomique et de Cosmologie, Université Grenoble-Alpes, CNRS/IN2P3, Grenoble F-38026, France

(Received 11 October 2017; published 20 June 2018)

Dark sectors lying beyond the Standard Model and containing sub-GeV particles which are bilinearly coupled to nucleons would induce quantum forces of the Casimir-Polder type in ordinary matter. Such new forces can be tested by a variety of experiments over many orders of magnitude. We provide a generic interpretation of these experimental searches and apply it to a sample of forces from dark scalars behaving as $1/r^3$, $1/r^5$, $1/r^7$ at short range. The landscape of constraints on such quantum forces differs from the one of modified gravity with Yukawa interactions and features, in particular, strong short-distance bounds from molecular spectroscopy and neutron scattering.

DOI: 10.1103/PhysRevD.97.115034

I. INTRODUCTION

When going beyond the Standard Model (SM) of particle physics, it is natural to imagine the existence of other light particles, which would have been so far elusive because of their weak or vanishing interactions with the SM particles. Such speculations on *dark sectors* could be simply driven by theoretical curiosity although there are more concrete motivations coming from two striking observational facts: dark matter and dark energy. In both cases, theoretical constructions elaborated to explain one or both of these fundamental aspects of the Universe tend to assume the existence of dark sectors of various complexity.

Among the many possibilities for the content of the dark sector, our interest in this work lies in dark particles with masses below the GeV scale, where quantum chromodynamics (QCD) reduces to an effective theory of nucleons. If a light scalar coupled to nucleons, it would induce a fifth force of the form $V = \alpha e^{-r/\lambda}/r$, with $\lambda = \hbar/mc$ being the Compton wavelength of the scalar and m its mass. The presence of such a Yukawa-like force is sometimes dubbed "modified gravity." Experimental searches for such fifth forces between nucleons extend from nuclear to astronomic scales and lead to a landscape of exclusion regions, see summary plots in [1–5].

As noted in [6], even in the absence of a light boson linearly coupled to nucleons, other fifth forces can still arise from the dark sector whenever a sub-GeV particle of any spin is bilinearly coupled to nucleons. Such forces would arise from the double exchange of a particle and are, thus, fundamentally quantum. Moreover, in order to take into account retardation effects, such forces have to be computed within relativistic quantum field theory. This kind of computation has been first done by Casimir and Polder for polarizable particles [7], and by Feinberg and Sucher for neutrinos [8]. We will refer to such quantum forces as Casimir-Polder forces.

There is a variety of motivations for having a particle of the dark sector coupling bilinearly to nucleons. The dark particle can be for instance charged under a symmetry of the dark sector, can be a symmetron from a dark energy model, or simply a dark fermion sharing a contact interaction with nucleons. Such Z_2 symmetry also can be needed in order to explain the stability of dark matter.

In the presence of forces which do not have a Yukawa-like behavior, as is the case of the Casimir-Polder forces we focus on, the landscape of fifth force searches is expected to change drastically. A thorough investigation of the experimental fifth force searches then becomes mandatory in order to put bounds on such extra forces in a consistent manner, and thus on the underlying dark particles.

This requires revisiting each of the experimental results, a task that will be performed in this paper. In Sec. II, we consider Casimir-Polder forces focussing on the case of a scalar with various effective interactions with nucleons. General features of Casimir-Polder forces are then derived

*philippe.brax@ipht.fr
†sylvain@ift.unesp.br
‡guillaume.pignol@lpsc.in2p3.fr

in Sec. III. A generic interpretation of the most recent and stringent fifth force searches, valid for arbitrary potentials, is given in Sec. IV. The exclusion regions will be displayed and discussed in Sec. V.

We emphasize that our approach to constrain dark sectors relies only on virtual dark particles, and is thus independent on whether or not the dark particle is stable. The case where the dark particle is stable and identified as dark matter has been treated in a dedicated companion paper, Ref. [6], where a complementarity with low-mass direct detection bounds (like XQC [9–11]) has been found. Searches for dark sectors via loops of virtual dark particles include Refs. [6,12,13], and are yet under-represented in the literature.

II. CASIMIR-POLDER FORCES FROM A DARK SCALAR

There are many reasons why the dark sector could feature a scalar with a Z_2 symmetry with respect to the Standard Model sector. If such a scalar is charged under a new symmetry such as a $U(1)_X$ charge while the SM fields are not, the scalar should interact with the SM via bilinear operators. The scalar can also be the pseudo-Nambu-Goldstone boson (pNGB) of an approximate global symmetry, in which case it couples mostly with derivative couplings to the nucleons. Theories of modified gravity can also feature light scalars with a bilinear coupling to the stress-energy tensor [14]. While the properties of these scalars are often considered to be modified by some screening mechanism, it is certainly relevant to consider scenarios where screening is negligible or absent. This is the most minimal possibility and can also serve as a reference for comparison with the screened models. Moreover, for models like the symmetrons, screening does not happen in vacuum.

All these possibilities of the dark sector can be UV-completed in a warped five-dimensional framework where the SM lies on the UV brane while the dark sector is on the IR brane and in the bulk. At energies larger than the KK scale μ, interactions between SM and dark sector become exponentially suppressed by $\sim e^{-E/\mu}$ and the SM is mostly ignorant of the dark sector—as first noted in [15] in another context. By AdS/CFT this framework is also equivalent to have a dark sector made of bound states from a strongly interacting theory with large number of color and conformal in the UV. Some details are given in Appendix A. This model will be the focus of a future publication [16].

It is convenient to use an effective field theory (EFT) approach to describe the interactions of the dark particle. All the measurements we consider occur well below the quantum chromodynamics (QCD) confinement scale; hence, we can readily write down effective interactions with nucleons. The operators we consider have the form $\mathcal{O}_{\rm nuc}\mathcal{O}_{\rm DS}$, where $\mathcal{O}_{\rm nuc}$ is bilinear in the nucleon fields and $\mathcal{O}_{\rm DS}$ is bilinear in the dark sector field. $\mathcal{O}_{\rm nuc}$ has in principle a $\bar{N}\Gamma^A N$ structure, where Γ^A can have any kind of Lorentz structure. In the limit of unpolarized nonrelativistic nucleons, only the interactions involving $\mathcal{O}_{\rm nuc} = \bar{N}N, \bar{N}\gamma^0 N$ are relevant, the other being either canceled by averaging over nucleon spins or suppressed by powers of m_N^{-1}.

In this paper, we focus on the exchange of a dark scalar. The exchange of dark fermions and dark vectors, either self-conjugate or complex, have been treated in [6], and details of the calculations for all these cases are given in Appendix B. Here, we focus on three types of effective interactions, $\mathcal{L} = \mathcal{L}_{\rm SM} + \mathcal{O}_i$, with

$$\mathcal{O}_a^0 = \frac{1}{\Lambda}\bar{N}N\frac{\phi^2}{2}, \qquad \mathcal{O}_b^0 = \frac{1}{\Lambda^2}\bar{N}\gamma^\mu N\phi^* i\overleftrightarrow{\partial}_\mu\phi,$$
$$\mathcal{O}_c^0 = \frac{1}{\Lambda^3}\bar{N}N\frac{(\partial^\mu\phi)^2}{2}. \tag{2.1}$$

We assume that only one of these operators is turned on at a time. In the $\mathcal{O}_{a,c}^0$ cases, we assume a real scalar, while for $\mathcal{O}_b^0$ we assume a complex scalar. The $\mathcal{O}_a^0$ interaction corresponds to the case of a symmetron, the $\mathcal{O}_b^0$ interaction is typically the one generated from a heavy Z' exchange, and the $\mathcal{O}_c^0$ would occur if the scalar is the pNGB of a hidden global symmetry. In the last case, as the pNGB mass explicitly breaks the shift symmetry, an interaction of the form $\frac{m^2}{\Lambda^2}\mathcal{O}_a^0$ could also be present. However, its effect would be negligible at short distance; hence, we do not take it into account. Similar calculations have been performed for disformal couplings in [17,18].

Higher-dimensional operators are in principle present in the effective Lagrangian, and are suppressed by higher powers of either Λ or $\Lambda_{\rm QCD}$. The EFT is valid for momenta below $\min(\Lambda, \Lambda_{\rm QCD})$ when coupling constants are $O(1)$ in the UV theory. We will assume a universal coupling to protons and neutrons—all our results are easily generalized for nonuniversal couplings. Also, for simplicity, we do not consider the dark particle coupling to electrons. Including the coupling to electrons would lead typically to stronger forces and thus to enhanced limits.

As a result of the $\mathcal{O}_{a,b,c}$ interactions, nucleons can exchange *two* scalars as shown in the Feynman diagram of Fig. 1. This Feynman diagram induces a Casimir-Polder

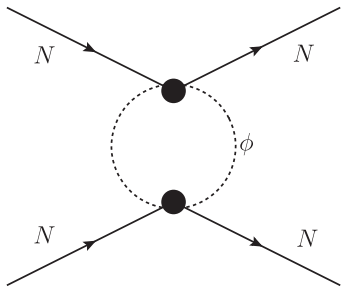

FIG. 1. The exchange of two scalars inducing a force between the nucleons.

force (*i.e.,* a relativistic van der Waals force) between the nucleons. The forces induced by the $\mathcal{O}_{a,b,c}$ operators have been computed in [6] and are given by the potentials

$$V_a = -\frac{1}{32\pi^3\Lambda^2}\frac{m}{r^2}K_1(2mr), \qquad V_b = \frac{1}{8\pi^3\Lambda^4}\frac{m^2}{r^3}K_2(2mr),$$
$$V_c = -\frac{1}{32\pi^3\Lambda^6 r}\left(\left(\frac{30m^2}{r^4}+\frac{6m^4}{r^2}\right)K_2(2mr) + \left(\frac{15m^3}{r^3}+\frac{m^5}{r}\right)K_1(2mr)\right), \tag{2.2}$$

where K_i is the ith modified Bessel function of the second kind. The V_a force is consistent with a previous calculation of [19] after matching to our conventions.

The main steps of the general calculation are as follows. One first calculates the amplitude corresponding to the diagram in Fig. 1. In order to calculate loop amplitudes in the EFT, dimensional regularization has to be used in order not to spoil the EFT expansion. The one-loop amplitudes can be decomposed over the basis

$$f_n = \int_0^1 dx(x(1-x))^n \log\left(\frac{\Delta}{\Lambda^2}\right), \tag{2.3}$$

where $\Delta = m^2 - x(1-x)q^2$. Λ is the scale at which the effective theory is matched on to the UV theory and is also the scale at which the EFT breaks down.

Then one takes the nonrelativistic limit of the amplitude and identifies the scattering potential $\tilde{V}$ as

$$i\mathcal{M} = -i\tilde{V}(|\mathbf{q}|)4m_N^2\delta^{s_1 s_1'}\delta^{s_2 s_2'}, \tag{2.4}$$

where $s_{1,2}$ ($s'_{1,2}$) corresponds to the spin polarization of each ingoing (outgoing) nucleons. The spatial potential is given by the three-dimensional Fourier transform of $\tilde{V}(|\mathbf{q}|)$,

$$V(r) = \int \frac{d^3\mathbf{q}}{(2\pi)^3}\tilde{V}(|\mathbf{q}|)e^{i\mathbf{q}\cdot\mathbf{r}} = \frac{-i}{(2\pi)^2 r}\int_{-\infty}^{\infty} d\rho\rho\tilde{V}(\rho)e^{i\rho r}, \tag{2.5}$$

where $r = |\mathbf{r}|$ and the momentum has been extended to the complex plane in the last equality, $\rho \equiv |\mathbf{q}|$. Using standard complex integration, one obtains

$$V(r) = \frac{-i}{(2\pi)^2 r}\int_{i2m}^{i\infty} d\rho\rho[\tilde{V}]e^{i\rho r} = \frac{i}{(2\pi)^2 r}\int_{2m}^{\infty} d\lambda\lambda[\tilde{V}]e^{-\lambda r}, \tag{2.6}$$

where $[V]$ is the discontinuity from right to left across the positive imaginary axis, $[V] = V_{\text{right}} - V_{\text{left}}$, and one has defined $\rho = i\lambda$. Notice that λ can also be understood as $\sqrt{t}$, the square root of the t Mandelstam variable extended to the complex plane. The discontinuities $[f_n]$ needed to compute the Casimir-Polder force via Eq. (2.6) are given in Appendix B.

In the case of the scalar dark particle exchanged via the $\mathcal{O}_a$, $\mathcal{O}_b$ or $\mathcal{O}_c$ operators, the amplitudes are given in Appendix C. The discontinuities needed to calculate the $V_{a,b,c}$ potentials are

$$[f_0] = i\pi\frac{2}{\lambda}\sqrt{\lambda^2-4m^2},$$
$$[f_1] = i\pi\frac{2m^2+\lambda^2}{3\lambda^3}\sqrt{\lambda^2-4m^2},$$
$$[f_2] = i\pi\frac{6m^4+2m^2\lambda^2+\lambda^4}{15\lambda^5}\sqrt{\lambda^2-4m^2}. \tag{2.7}$$

The discontinuity of the nonrelativistic scattering potentials for the three diagrams considered above are

$$[\tilde{V}_a] = \frac{[f_0]}{32\pi^2\Lambda^2},$$
$$[\tilde{V}_b] = \frac{m^2[f_0]-\lambda^2[f_1]}{8\pi^2\Lambda^4},$$
$$[\tilde{V}_c] = \frac{(6m^4+m^2\lambda^2)[f_0]+(24m^2\lambda^2+\lambda^4)[f_1]+20\lambda^4[f_2]}{64\pi^2\Lambda^6}. \tag{2.8}$$

At short distance $mr \ll 1$ the forces behave as

$$V_a = -\frac{1}{64\pi^3\Lambda^2 r^3}, \qquad V_b = \frac{1}{16\pi^3\Lambda^4 r^5},$$
$$V_c = -\frac{15}{32\pi^3\Lambda^6 r^7}, \tag{2.9}$$

while at long distance $mr \gg 1$, the forces go as

$$V_a = -\frac{\sqrt{m}e^{-2mr}}{64\pi^{5/2}\Lambda^2 r^{5/2}}, \qquad V_b = \frac{m^{3/2}e^{-2mr}}{16\pi^{5/2}\Lambda^4 r^{7/2}},$$
$$V_c = -\frac{m^{9/2}e^{-2mr}}{64\pi^{5/2}\Lambda^6 r^{5/2}}. \tag{2.10}$$

As sketched in [6], the broad features of these forces can be understood from general principles. The arguments are given in detail in the next section.

III. GENERAL CONSIDERATIONS ON CASIMIR-POLDER FORCES

A. Structure of the effective theory

Let us first comment on the effective theory giving rise to the Casimir-Polder forces. The four-nucleon loop diagrams we consider come from higher-dimensional operators and are thus more divergent than the four-nucleon diagrams from the UV theory lying above Λ. This implies

that four-nucleon *local* operators (*i.e.,*. counterterms) of the form $(\bar{N}N)^2$, $(\partial^\mu(\bar{N}N))^2$, … are also present in the effective Lagrangian to cancel the divergences which are not present in the UV theory. The finite contribution from these local operators is fixed by the UV theory at the matching scale, and is expected to be of same order as the coefficient of the $\log\Lambda$ term in the amplitude by naive dimensional analysis (this situation is analog to renormalization of the nonlinear sigma model; see Ref. [20]). The loop amplitudes have the form

$$\mathcal{M} = F(q^2) + G(q^2)\log\left(\frac{m}{\Lambda}\right), \tag{3.1}$$

where $F(q^2)$ is complex, with $F(q^2=0)=0$, and $G(q^2)$ is a real polynomial in q^2 (both depend also on m, Λ). The log term is a consequence of the divergence. The log term is real and contributes to the running of local four-nucleon operators. The Casimir-Polder force arises from the branch cut of $F(q^2)$ and is, thus, independent of the log term. An experiment measuring only the Casimir-Polder force will have the advantage of being insensitive to these four-nucleon operators, which are set by the UV completion and, thus, introduce theoretical uncertainty. This happens either when the experiment is nonlocal by design (*e.g.,*. measuring the force between nucleons at a nonzero distance), or by construction of the observables as we will see in the case of neutron scattering. All the measurements considered in this paper are either fully or approximately insensitive to local four-nucleon interactions.

Certain of the experiments we are considering (namely molecular spectroscopy and bouncing neutrons) rely on systems which are small enough to necessitate a quantum description of the nucleus. The wave functions associated to the quantum states in these systems are computed using QED and are, thus, valid down to an internuclear distance of order the radius of the nucleus $r \sim r_{\rm nuc}$, with typically $r_{\rm nuc}^{-1} = O(100\ \text{MeV})$. These wave functions will be convoluted with the potential of the dark force, hence the space integral should be cut off at a value $r_{\rm UV}$ given by the maximum of $r_{\rm nuc}$ and the inverse cutoff of the EFT. Depending on the behavior of the wave function and of the dark force at small r, the observables can be sensitive to $r_{\rm UV}$ or not. Having a cutoff-dependent observable is not inconsistent, and often occurs in high-energy physics, for instance when loop contributions to electroweak observables are computed. The $r < r_{\rm UV}$ contribution to the space integrals are not computed. When the observable is independent of $r_{\rm UV}$, one may expect that the $r < r_{\rm UV}$ contribution to the integral is negligible. On the other hand, when the observable is cutoff dependent, it is likely that physics beyond $r < r_{\rm UV}$ contribute as well. In such case, the predictions from the $r > r_{\rm UV}$ piece of the integral should be understood as mere estimates.

B. General features of Casimir-Polder forces

The main features of Casimir-Polder forces between two nonrelativistic sources can be understood using dimensional analysis and the optical theorem. We focus on the double exchange of a particle having local interactions with the sources, the operators used in Sec. II being examples of such a scenario. We further assume that the sources are identical—a similar approach applies similarly to different sources. We denote by X the dark particle exchanged, $\bar{X}$ its conjugate, m its mass. We use nucleons as source for concreteness. X can take any spin. The generic operator we consider has the form

$$\mathcal{L} \supset \frac{1}{\Lambda^n}\mathcal{O}(X)\bar{N}\Gamma^A N, \tag{3.2}$$

where Γ^A can be any Lorentz structure. When averaging over the nucleon spins, the first nonvanishing Lorentz structures are $\bar{N}N$ ("scalar channel"), $\bar{N}\gamma^\mu N$ ("vector channel"), and we will focus on those ones.

Within the above assumptions we obtain the following properties:

(i) *Sign.* Operators of the form $\mathcal{O}(X)\bar{N}N$ give rise to attractive forces. Operators of the form $\mathcal{O}_\mu(X)\bar{N}\gamma^\mu N$ give rise to repulsive forces.

(ii) *Short distance.* An operator of dimension $n+4$ gives rise to a potential behaving at short distance as

$$V(r) \propto \frac{1}{r^{1+2n}}. \tag{3.3}$$

(iii) *Long distance.* When the square amplitude $|\mathcal{M}(N\bar{N}\leftrightarrow X\bar{X})|^2$ taken at $\sqrt{s}\sim 2m$ is suppressed by a power $(s-4m^2)^p$ (*i.e.,* velocity-suppressed by v^{2p}), the long range behavior of the force is given by

$$V(r) \propto \frac{e^{-2mr}}{r^{\frac{5}{2}+p}}. \tag{3.4}$$

Let us prove the above properties. Property 2 is simply a consequence of dimensional analysis. When $r \ll 1/m$, the potential can be expanded with respect to rm and at first order, $V(r) = V(r)|_{m=0}(1+O(mr))$. In this limit the potential depends only on r and on the effective coupling $1/\Lambda^n$ squared. The potential having dimension one, it must have a dependence in $1/r^{2n+1}$ so that dimensions match. Notice that this argument applies similarly for the exchange of a single particle (giving then a $1/r$ potential) or for the exchange of an arbitrary number of particles.

For Properties 1 and 3, let us denote the amplitude of interest (Fig. 1) by $i\mathcal{M}_t$, and introduce the amplitude $i\mathcal{M}_s = i\mathcal{M}(N\bar{N}\to X^*\bar{X}^*\to N\bar{N})$, which is the $s\leftrightarrow t$ crossing of $i\mathcal{M}_t$. In order to get some insight on $i\mathcal{M}_t$, we can study $i\mathcal{M}_s$ use crossing symmetry. The optical theorem applies to $i\mathcal{M}_s$, with

$$\begin{aligned}\mathrm{Im}(\mathcal{M}_s) &= \mathrm{Im}(\mathcal{M}(N\bar{N} \to X^*\bar{X}^* \to N(q_1)\bar{N}(q_2))) \\ &= \frac{1}{2}\sum_{\text{polar}} \int \frac{d^4q_1}{(2\pi)^3}\delta(q_1^2)\frac{d^4q_2}{(2\pi)^3}\delta(q_2^2)(2\pi)^4\delta^4(q_1+q_2-q)|\mathcal{M}(N\bar{N} \to X(q_1)\bar{X}(q_2))|^2 \\ &= \frac{1}{16\pi}\sqrt{1-\frac{4m^2}{s}}\sum_{\text{polar}}|\mathcal{M}(N\bar{N} \to X(q_1)\bar{X}(q_2))|^2 \end{aligned} \tag{3.5}$$

where in the last line we use the fact that the amplitude arising from local interactions [Eq. (2.6)] depend only on the center-of-mass energy $\sqrt{s}$. The optical theorem is of interest because $\mathrm{Im}(\mathcal{M}_t)$ is directly related to the discontinuity of $\mathcal{M}_t$ over its branch cut, which is precisely the quantity needed to calculate nonrelativistic potential. In the formalism of Sec. II, we have

$$\mathrm{Im}(\mathcal{M}_t) = -2[\tilde{V}]m_N^2\delta^{s_1s_2}\delta^{s_1's_2'}. \tag{3.6}$$

It turns out that $\mathrm{Im}(\mathcal{M}_t) > 0$ (< 0) corresponds to an attractive (repulsive) force.

Let us prove Property 1. For the scalar channel, the crossing of $\mathrm{Im}(\mathcal{M}_s)$ stays positive, hence $\mathrm{Im}(\mathcal{M}_t) > 0$ and the force is attractive. For the vector channel, we have $\mathcal{M}(N\bar{N} \to X\bar{X}) \propto J_{\mu,N}J_X^\mu$ where the J_μ are vector currents. The square matrix elements takes the form $(J_{\mu,N}J_{\nu,N})(J_{\mu,X}J_{\nu,X})$. All the J_μ are conserved currents, $J_\mu q^\mu = 0$. The $J_{\mu,N}$ can be pulled outside of the integral in Eq. (3.5). Conservation of the $J_{\mu,N}$ currents implies that they project out the components proportional to q_μ of the quantity they are contracted with. It follows that

$$J_{\mu,N}J_{\nu,N}\sum_{\text{polar}}(J_{\mu,X}J_{\nu,X}) = J_{\mu,N}J_{\nu,N}A(s)(q^\mu q^\nu - sg^{\mu\nu}), \tag{3.7}$$

where we have introduced $s = (q_1+q_2)^2$ and $A(s)$ is a positive function. In the nonrelativistic limit, one keeps only the $\mu = \nu = 0$ components of the nucleon currents, and the projector reduces to $q^\mu q^\nu - sg^{\mu\nu} \sim \mathbf{q}^2$—hence $A(s)$ has to be positive to ensure $\mathrm{Im}(\mathcal{M}_s) > 0$. The crossing of $\mathrm{Im}(\mathcal{M}_s)$ gives

$$\mathrm{Im}(\mathcal{M}_t) = (\tilde{J}_{\mu,N}\tilde{J}_{\nu,N})A(t)(q^\mu q^\nu - tg^{\mu\nu}), \tag{3.8}$$

where $\tilde{J}_{\mu,N}$ denotes the crossed nucleon currents. In the nonrelativistic limit, we have $\tilde{J}_{\mu,N}\tilde{J}_{\nu,N} \sim 4m_N^2\delta^{\mu0}\delta^{\nu0}\delta^{s_1s_2}\delta^{s_1's_2'}$, $q^0 \sim 0$, $t \sim -\mathbf{q}^2$. However, when taking the Fourier transform of $\tilde{V}(\mathbf{q})$ [see Eq. (2.6)], $|\mathbf{q}|$ is extended to the complex plane. The nonrelativistic potential is then given by an integral of $\mathrm{Im}(\mathcal{M}_t)$ over positive values of the *real* variable λ, which is related to t by $\lambda \equiv \sqrt{t}$. Hence the t variable in Eq. (3.8) is positive when computing the nonrelativistic potential. This implies that $\mathrm{Im}(\mathcal{M}_t)$ is always negative, and thus the Casimir-Polder force between nucleons induced by a vector channel is always repulsive.

Let us finally prove Property 3. We first remark that the long distance behavior of the $V(r)$ potential amounts to having a steep exponential in $\int_{2m}^{\infty} d\lambda\lambda[\tilde{V}]e^{-\lambda r}$, see Eq. (2.6). When this is true we are allowed to expand $[\tilde{V}]$ as a power series at small values of λ, hence at the point $\lambda = 2m$. In order to understand what form this power series takes, let us consider the square amplitude $|\mathcal{M}(N\bar{N} \leftrightarrow X\bar{X})|^2$, which corresponds to pair production or annihilation of X. This amplitude arises from the local operators of Eq. (2.6) hence it depends only on the center-of-mass energy $\sqrt{s}$. We extend s to the complex plane. We can always perform a power series expansion near $s = 4m^2$,[1]

$$\begin{aligned}&|\mathcal{M}(N\bar{N} \leftrightarrow X\bar{X})|^2 \\ &\quad = 4m_N^2(a + b(s-4m^2) + c(s-4m^2)^2 + \ldots)\end{aligned} \tag{3.9}$$

where the $4m_N^2$ factor is introduced for further convenience and the a, b, c are dimensionful constants. Using the optical theorem, we obtain that

$$\begin{aligned}\mathrm{Im}(\mathcal{M}_s) = \frac{m_N^2}{4\pi^2}\sqrt{1-\frac{4m^2}{s}}&(a + b(s-4m^2) \\ &+ c(s-4m^2)^2 + \ldots),\end{aligned} \tag{3.10}$$

and crossing then gives

$$\begin{aligned}\mathrm{Im}(\mathcal{M}_t) = \frac{m_N^2}{4\pi^2}\sqrt{1-\frac{4m^2}{t}}&(a + b(t-4m^2) \\ &+ c(t-4m^2)^2 + \ldots).\end{aligned} \tag{3.11}$$

[1]Note that the quantity $\frac{\sqrt{s-4m^2}}{4m} = \frac{\mathbf{q}}{m} \equiv v$ taken in the center-of-mass frame is the usual velocity of the X particle. It is common to say that the squared matrix-element is "velocity-suppressed" when *e.g.*, $a = 0$. The nucleons being by assumption heavier than X, neither production nor annihilation of X can physically happen at this threshold. However, formally, nothing forbids us to perform the expansion.

$\mathrm{Im}(\mathcal{M}_t)$ is related to $[\tilde{V}]$ by Eq. (3.6) and $[\tilde{V}]$ is related to $V(r)$ by Eq. (2.6). The potential in the long range limit turns out to be[2]

$$V(r) = -\frac{1}{32\pi^{5/2}} e^{-2mr}\left(a\frac{m^{1/2}}{r^{5/2}} + b\frac{6m^{3/2}}{r^{7/2}} + c\frac{60m^{5/2}}{r^{9/2}} + \ldots\right). \tag{3.13}$$

We can see that an extra factor of $1/r$ in $V(r)$ is associated to each factor of $s - 4m^2$ in the expansion of $|\mathcal{M}(N\bar{N} \leftrightarrow X\bar{X})|^2$.

IV. FIFTH FORCE SEARCHES

This section describes how to interpret the results of a number of experiments as bounds on an arbitrary fifth force.

A. Neutron scattering

Progress in measuring the scattering of cold neutrons off nuclei have been recently made and have been used to put bounds on short-distance modified gravity, [21–28]. The cold neutron scattering cross section can be measured at zero angle by "optical" methods, at nonzero angles using Bragg diffraction, or over all angles by the "transmission" method giving then the total cross section [29].

In the following, we adapt the analyses of [27] to the Casimir-Polder forces of Eq. (2.2). At low energies the standard neutron-nuclei interaction is a contact interaction in the sense that it can be described by a four-fermion operator $\mathcal{O}_{4N} = (\bar{N}N)^2$.[3,4] New physics can in general induce both contact and noncontact contributions to the neutron-nuclei interaction. A noncontact contribution vanishes at zero momentum, while a contact contribution remains non-null and can be described by $\mathcal{O}_{4N}$. It is convenient to introduce the scattering length

$$\sqrt{\frac{\sigma(\mathbf{q})}{4\pi}} \equiv l(\mathbf{q}) = l^{\mathrm{C}}_{\mathrm{std}} + l^{\mathrm{C}}_{\mathrm{NP}} + l^{\mathrm{NC}}_{\mathrm{NP}}(\mathbf{q}), \tag{4.1}$$

where the $l^{\mathrm{C}}_{\mathrm{std}}$, $l^{\mathrm{C}}_{\mathrm{NP}}$ local terms are independent of momentum transfer $\mathbf{q}$ and $l^{\mathrm{NC}}_{\mathrm{NP}}(\mathbf{q})$, which satisfies $l^{\mathrm{NC}}_{\mathrm{NP}}(\mathbf{q} = 0) = 0$, is the noncontact contribution. The $l^{\mathrm{NC}}_{\mathrm{NP}}(\mathbf{q})$ term contains the Casimir-Polder force (see Sec. III), and log terms of the form $|\mathbf{q}|^{2n}\log(m/\Lambda)$. The new physics contribution $l_{\mathrm{NP}}(\mathbf{q})$ is related to the scattering potential $\tilde{V}$ by $l_{\mathrm{NP}}(\mathbf{q}) = 2m_N\tilde{V}(\mathbf{q})$, which is just the Born approximation.[5]

For the forces described in Eq. (2.2), the new physics contributions are given by

$$l_a(|\mathbf{q}|^2) = \frac{m_N}{16\pi^2\Lambda^2} f_0, \tag{4.2}$$

$$l_b(|\mathbf{q}|^2) = \frac{m_N}{4\pi^2\Lambda^4}(m^2 f_0 + |\mathbf{q}|^2 f_1), \tag{4.3}$$

$$l_c(|\mathbf{q}|^2) = \frac{m_N}{16\pi^2\Lambda^6}\left(\left(3m^4 - \frac{m^2|\mathbf{q}|^2}{2}\right)f_0 + \left(\frac{|\mathbf{q}|^4}{2} - 12m^2|\mathbf{q}|^2\right)f_1 + 10|\mathbf{q}|^4 f_2\right), \tag{4.4}$$

where the f_n are the loop functions defined Eq. (2.3). A convenient way to look for an anomalous interaction is to search for $l^{\mathrm{NC}}_{\mathrm{NP}}(\mathbf{q})$ by comparing the scattering length obtained by different methods, using for instance $l_{\mathrm{Bragg}} - l_{\mathrm{opt}}$, $l_{\mathrm{tot}} - l_{\mathrm{opt}}$. This approach eliminates the contact contributions $l^{\mathrm{C}}_{\mathrm{std}}$ and $l^{\mathrm{C}}_{\mathrm{NP}}$, and is, therefore, only sensitive to $l^{\mathrm{NC}}_{\mathrm{NP}}(\mathbf{q})$.

(i) *Optical + Bragg.*—One approach is to compare the forward and backward scattering lengths measured respectively by optical and Bragg methods. Using the analysis from [27], one has a 95% CL bound

$$\frac{1}{2m_N}(l_i(0) - l_i(k^2_{\mathrm{Bragg}})) < (0.01\ \mathrm{fm})^2, \tag{4.5}$$

with $k_{\mathrm{Bragg}} = 2$ keV.

(ii) *Optical + total cross section.*—The total cross section measured by the transmission method provides the average scattering length

$$\bar{l}_i(k) = \frac{1}{2}\int_0^\pi d\theta \sin(\theta) l_i(4k^2\sin^2(\theta/2)). \tag{4.6}$$

Using information from optical method measurement, we have the 95% CL bound

$$l_i(0) - \bar{l}_i(k_{\mathrm{ex}}) < 6\times 10^{-4}\ \mathrm{fm}, \tag{4.7}$$

with $k_{\mathrm{ex}} = 40$ keV.

For both methods, a dependence on the $|\mathbf{q}|^{2n}\log(m/\Lambda)$ remains, which turns out to be mild in practice. Hence, our results are still approximatively independent of the local

[2]The general case is obtained similarly using the identity

$$\int_{2m}^{\infty} d\lambda\lambda(\lambda^2 - 4m^2)^{\frac{1}{2}+p} = \left(\frac{4m}{r}\right)^{p+1}\frac{\Gamma(3/2+p)}{\sqrt{\pi}}K_{p+1}(2mr). \tag{3.12}$$

[3]Various contact operators can be written when differentiating between neutrons and protons. However, this is not crucial for the discussion hence we use only "N," which refers to both protons and neutrons.

[4]As described in [27], there is also a small electromagnetic dipole interaction, which is taken into account in the analysis and which we do not discuss here.

[5]We emphasize that no extra theoretical assumptions have been made above, this formalism is a mere rewriting of the scattering amplitude to highlight the important features and to put it in a form more common to neutron experiments.

four-nucleon operators, which are fixed by the unspecified UV completion (see Sec. III).

B. Molecular spectroscopy

Impressive progress on both the experimental [30–37] and the theoretical [38–49] sides of precision molecular spectroscopy have been accomplished in the past decade, opening the possibility of searching for extra forces below the Å scale using transition frequencies of well-understood simple molecular systems. Certain of these results have recently been used to bound short distance modifications of gravity, see Refs. [5,50–52].

The most relevant systems for which both precise measurements and predictions are available are the hydrogen molecule H_2, the molecular hydrogen-deuterium ion HD^+ and muonic molecular deuterium ion $dd\mu^+$, where d is the deuteron. This last system is exotic in the sense that a heavy particle, the muon, has been substituted for an electron. As a result the internuclear distances are reduced, providing a sensitivity to forces of shorter range, and thus to heavier dark particles.

The presence of an extra force shifts the energy levels by

$$\Delta E_i = \int d^3\mathbf{r}\Psi^*(r)V_i(r)\Psi(r) \tag{4.8}$$

at first order in perturbation theory. We have computed these energy shifts for the transitions between the $(\nu = 1, J = 0) - (\nu = 0, J = 0)$ states for H_2, the $(\nu = 4, J = 3) - (\nu = 0, J = 2)$ states of HD^+, and the binding energy of the $((\nu = 1, J = 0))$ state of $dd\mu^+$ using the wave functions given in [5,51]. ν and J are respectively the rotational and vibrational quantum numbers. For the quantum states considered here, the typical internuclear distances are $\sim$1 Å for H_2 and HD^+, and $\sim$0.005–0.08Å for $dd\mu^+$.

The wave functions of these states are shown in Appendix D. The bounds on the extra forces are obtained by asking that ΔE be smaller than the combined uncertainties given by $\delta E = \delta E^{\rm exp} \oplus \delta E^{\rm th}$. These experimental and theoretical uncertainties are summarized in Table I, and more details can be found in the original references. For the transition energies, the experimental uncertainties are larger than the theoretical ones by a factor of $O(1)$ to $O(10)$. For the binding energy of the $dd\mu^+$ ground state, the experimental uncertainty dominates by a $O(10)$ factor.

TABLE I. Experimental and theoretical uncertainties for molecular observables (transition or bin-ding energies) considered in this work.

	$\delta E^{\rm exp}$	$\delta E^{\rm th}$
H_2 $(\nu = 1, J = 0) - (\nu = 0, J = 0)$ [50,51]	3.0 neV	1.5 neV
HD^+ $(\nu = 4, J = 3) - (\nu = 0, J = 2)$ [50]	0.33 neV	0.044 neV
$dd\mu^+$ $(\nu = 1, J = 0)$ [5]	0.7 meV	< 0.1 meV

At small r, the wave functions of these states are constant except for $dd\mu^+$ which behaves as $\sim r$ [53]. In all cases but for the $(\nu = 1, J = 0)$ states of $dd\mu^+$, the wave function at small r is so small that it is neglected—and its value is even difficult to obtain numerically [51,53]. On the other hand for $dd\mu^+$ the tail at small r is not negligible. For a force in $1/r^5$ (resp. $1/r^7$) the predicted energy shift depends on $\log(r_{\rm UV})$ (resp. $1/r_{\rm UV}^2$). We have taken $r_{\rm UV}$ to be the radius of the deuteron, which is of order 2×10^{-5} Å. To get a concrete idea of the dependence on the choice of the cut-off scale $r_{\rm UV}$, one can compare with the result obtained when cutting the wave function at a larger distance, taking as an example $r_{\rm UV} = 10^{-3}$ Å. In terms of the sensitivity to Λ, we get that the change is $O(10\%)$ for the $1/r^5$ force, and of a factor $\sim$4 for the $1/r^7$ force. In the latter case, this follows from the $1/r_{\rm UV}^2\Lambda^6$ dependence of the short distance contribution to energy levels, which is the dominant one, unlike in the other cases considered, and for which a change of $r_{\rm UV}$ by a factor of 50 leads to a change in Λ of order $50^{1/3} \sim 4$.

C. Experiments with effective planar geometry

A variety of experiments searching for new forces at submillimeter scales are measuring the attraction between two dense objects with typically planar or spherical geometries. Whenever the distance between the objects is small with respect to their size, these objects can be effectively approximated as infinite plates, and the force becomes proportional to the potential energy between the plates. This is the proximity force (or Derjaguin's) approximation [54]. An important subtlety is that most of the experiments are using objects coated with various layers of dense materials, that should be taken into account in the computation of the force. Thus, we end up with calculating the potential between two plates with various layers of density for each. The effective plane-on-plane geometries are summarized in Table II. It is convenient to describe all these configurations at once using a piecewise mass density function describing n layers over a bulk with density ρ,

$$\gamma_n(z) = \begin{cases} \rho_n & \text{if } 0 < z < \Delta_n \\ \rho_{n-1} & \text{if } 0 < z < \Delta_n + \Delta_{n-1} \\ \vdots & \\ \rho & \text{if } z > \sum_i^n \Delta_i. \end{cases} \tag{4.9}$$

In this notation, the layer labelled n is the closest to the other plate. The potential between an infinite plate of density structure $\gamma_a(z)$ and a plate with area A and density structure $\gamma_b(z)$ at a distance s is then given by

$$V_i^{\rm plate} = 2\pi A \int_0^\infty d\rho\rho \int_0^\infty dz_a\gamma(z_a) \int_0^\infty dz_b\gamma(z_b) \times V_i\left(\sqrt{\rho^2 + (s + z_a + z_b)^2}\right). \tag{4.10}$$

TABLE II. Summary of the fifth forces experiments with effective planar geometry used in this work. The reported densities which differ from the nominal ones given in Table III are indicated in parentheses.

Experiment	Plane a			Separation	Plane b			
Stanford [55]	–		Au, 30 μm	25 μm	Au			
IUPUI [56]	Sapphire	Cr, 10 nm	Au, 250 nm	[30–8000] nm	Au, 250 nm	Cr, 10 nm	Si, 2.1 μm Au, 2.1 μm	SiO_2
Lamoreaux [54,57]	$SiO_2^{(2.23)}$	Cu, 0.5 μm	Au, 0.5 μm	[0.6, 6] μm	Au, 0.5 μm	Cu, 0.5 μm	$SiO_2^{(2.40)}$	
AFM [54,58]	Polystyrene		$Au^{(18.88)}$, 86.6 nm	[62, 350] nm	$Au^{(18.88)}$, 86.6 nm		Sapphire	
μ-oscillator [54,59,60]	$Sapphire^{(4.1)}$	Cr, 10 nm	Au, 180 nm	[180, 450] nm	Au, 210 nm	Cr, 10 nm	Si	
Casimirless [54,60,61]	Sapphire	Cr, 1 nm	Au, 200 nm	[150, 500] nm	Au, 150 nm	Pt, 1 nm	Ge, 200 nm Au, 200 nm	Ti, 1 nm Si

TABLE III. Densities of the materials used in the fifth force experiments listed in Table II.

	Polyester	SiO_2	Si	Sapphire	Ti	Ge	Cr	Cu	Au
ρ [g cm^{-3}]	1.06	2.23	2.33	3.98	4.51	5.32	7.14	8.96	19.32
ρ [$10^6 \cdot$ keV^4]	4.75	9.99	1.04	1.78	2.02	2.38	3.20	4.01	8.66

In practice, most of these sub-millimeter experiments have released their results as bounds on a Yukawa-like force. In order to obtain consistent bounds on the strength of the Casimir-Polder forces Λ as a function of the scalar mass m, we have to compare the plane-on-plane potentials from the Casimir-Polder forces to the plane-on-plane potential from the Yukawa force. Bounds on the (α, m) parameters of the Yukawa force can be then translated into bounds on the (Λ, m) parameters of the Casimir-Polder forces, using the limit-setting procedure provided by each experiment.

The plane-on-plane potential for the Yukawa force is straightforward to compute analytically and reads

$$V_{\rm Yuk}^{\rm plate} = 2\pi A \frac{1}{m^3} e^{-ms} K_n^a K_{n'}^b,$$
$$K_n = \rho_n + \sum_{l=1}^{n} (\rho_{l-1} - \rho_l) \exp\left(-m \sum_{i=1}^{l} \Delta_{n-i+1}\right) \qquad (4.11)$$

with $\rho_0 = \rho$. In the case of the Casimir-Polder forces shown in Eq. (2.2), the triple integral of Eq. (4.10) are much less trivial to carry on analytically. A numerical integration is, however, easily done.

It is worth noticing that the z-integrals on the Casimir-Polder potentials can be realized using a different representation for the potentials, which naturally occurs when calculating the diagram of Fig. 1 in a mixed position-momentum space formalism, which we will extensively use in future work [62].

D. Bouncing neutrons

New forces can also be probed using bouncing ultracold neutrons (i.e., neutrons with velocities of a few m/s) [63–67]. The vertical motion of a neutron bouncing above a mirror nicely realizes the situation of a quantum point particle confined in a potential well, the gravitational potential $m_N g z$ pulling the neutron down, and the mirror pushing the neutron up. The properties of the discrete stationary quantum states for the bouncing neutron can be calculated exactly. The wave function of the $k^{\rm th}$ state reads

$$\psi_k(z) = C_k {\rm Ai}(z/z_0 - \epsilon_k), \qquad (4.12)$$

where Ai is the Airy function, ϵ_k is the sequence of the negative zeros of Ai and $z_0 = (2m_N^2 g/\hbar^2)^{-1/3} \approx 6$ μm. The first wave functions are shown in Appendix D. The theoretical energies of the quantum states are

$$E_k = m_N g z_0 \epsilon_k = \{1.41, 2.46, 3.21, 4.08, \ldots\} \text{ peV}. \qquad (4.13)$$

Recently, a measurement of the energy difference $E_3 - E_1$ was performed at the Institut Laue Langevin in Grenoble using a resonance technique [68]. The result is in agreement with the theoretical predictions. From this experiment a bound can be set on any new force which would modify the energy levels, the experimental precision being

$$\delta(E_3 - E_1) < 10^{-14} \text{ eV}. \qquad (4.14)$$

Let us calculate the energy shift due to the new Casimir-Polder dark force. The additional potential of a neutron at a height z above a semi-infinite glass mirror is given by

$$V_{i,z}(z) = 2\pi \frac{\rho_{\rm glass}}{m_N} \int_z^\infty dz' \int_0^\infty \rho d\rho V_i(r) \qquad (4.15)$$

where $\frac{\rho_{\rm glass}}{m_N} = 10^{10}$ eV^3 is the number density of nucleons in the glass, $V_i(r)$ is the potential between the neutron and one nucleon at a distance $r = \sqrt{\rho^2 + z'^2}$. The double integral in the expression of the potential can be simplified to a single integral:

$$V_{i,z}(z) = 2\pi \frac{\rho_{\rm glass}}{m_N} \int_z^\infty r(r-z) V_i(r) dr. \tag{4.16}$$

In the case of the potentials V_a and V_b, the integrals cannot be calculated analytically. However, we found suitable analytical approximations having the correct asymptotic behavior at zero and infinite height,

$$\begin{aligned} V_{a,z}(z) &= -\frac{\rho_{\rm glass}}{m_N} \frac{1}{32\pi^2\Lambda^2} \int_{2mz}^\infty \frac{u-2mz}{u} K_1(u) du \\ &\approx -\frac{\rho_{\rm glass}}{m_N} \frac{1}{32\pi^2\Lambda^2} \frac{K_0(2mz)}{1+2mz}, \end{aligned} \tag{4.17}$$

and

$$\begin{aligned} V_{b,z}(z) &= \frac{\rho_{\rm glass}}{m_N} \frac{m^2}{4\pi^2\Lambda^4} \int_{2mz}^\infty \frac{u-2mz}{u^2} K_2(u) du \\ &\approx \frac{\rho_{\rm glass}}{m_N} \frac{m^2}{4\pi^2\Lambda^4} \frac{K_1(2mz)}{2mz(3+2mz)}. \end{aligned} \tag{4.18}$$

The approximate expressions have a relative precision of better than 50% for $V_{a,z}$ and better than 3% in the case of $V_{b,z}$, for all values of z. The case of $V_{c,z}$ remains to be done.

Using the approximate expressions, we have computed the shift in the energy levels of the neutron quantum bouncer using first order perturbation theory:

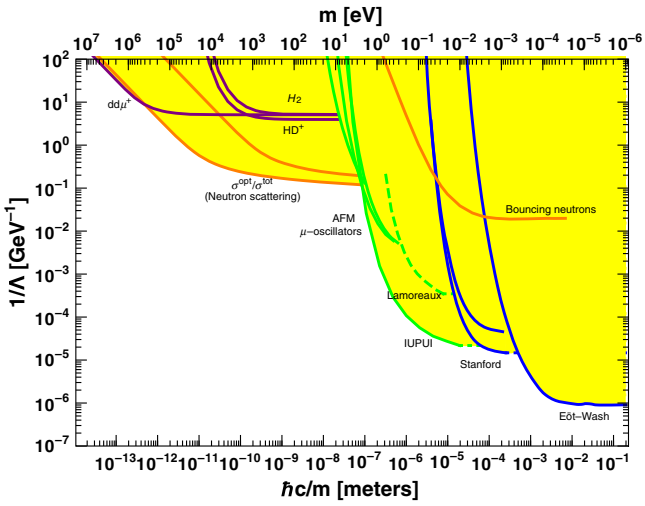

FIG. 2. Bounds on a scalar coupled to nucleons via the $\mathcal{O}_a$ interaction. The yellow region is excluded at 95% CL. See Sec. IV for details on exclusion regions.

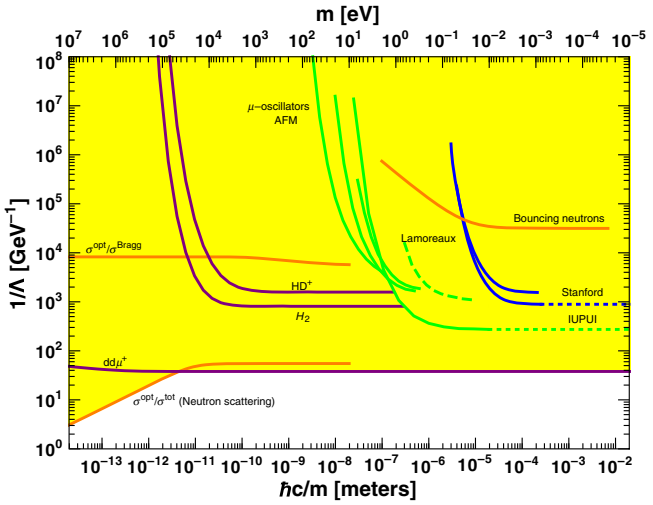

FIG. 3. Bounds on a scalar coupled to nucleons via the $\mathcal{O}_b$ interaction. Same conventions as Fig. 2.

$$\delta E_k = \int_0^\infty |\psi_k(z)|^2 V_z(z) dz. \tag{4.19}$$

These predictions are UV-insensitive. The bounds on the extra forces V_a and V_b as a function of the mediator mass m are obtained from the experimental constraint (4.14). They are reported in Figs. 2 and 3.

E. Moon perihelion precession

The existence of a fifth force at astrophysical scales would imply a slight modification of planetary motions. Any such fifth force can be treated perturbatively whenever it is small with respect to gravity at the distance between the two bodies. The modification of the equation of motion implies, among other effects, an anomalous precession of the perihelion of the orbit. In the case of the Moon, this precession is experimentally measured to high precision by lunar laser ranging experiments [69].

The fundamental Casimir-Polder forces of Eq. (2.2) are between two nucleons. For macroscopic bodies, the potentials are given by $\frac{m_1 m_2}{m_N^2} V_i$. Let us calculate the planetary motion in the presence of these new forces. We follow the formalism of Ref. [1]. The radial component of the Casimir-Polder forces between Earth and Moon is given by $F_i(r) = -\frac{m_{\mathbb{C}} m_\oplus}{m_N^2} \partial_r V_i(r)$. Introducing $u = \frac{1}{r}$, the Earth-Moon orbital equation reads

$$\frac{d^2u}{d\theta^2} + u = \frac{m_{\mathbb{C}}^2}{L^2 u^2} (m_{\mathbb{C}} m_\oplus G u^2 - F_i(1/u)), \tag{4.20}$$

where $L \equiv m_{\mathbb{C}} r^2 \frac{d\theta}{dt}$ is the conserved angular momentum and the first term in the parenthesis is the gravitational force. The solution of the unperturbed equation reads

$$u(\theta) = u_{\mathbb{C}}(1 + \epsilon\cos(\theta - \theta_0)), \quad u_{\mathbb{C}} = \frac{m_{\mathbb{C}}^3 m_\oplus G}{L^2}, \tag{4.21}$$

where ϵ is the orbital eccentricity ($\epsilon = 0.0549$ for the Moon), θ_0 indicates the perihelion of the ellipse, and the major semiaxis $a_{\mathbb{C}}$ is given by $a_{\mathbb{C}}^{-1} = u_{\mathbb{C}}(1 - \epsilon^2)$. At first order in perturbation theory, the extra force is just as a constant, $F_i(1/a_{\mathbb{C}})$, which only modifies $u_{\mathbb{C}}$, the overall size of the orbit. At second order in perturbation theory, one has

$$F_i(1/u) = F_i(1/a_{\mathbb{C}}) + \left(u - \frac{1}{a_{\mathbb{C}}}\right)\frac{\partial F_i(1/u)}{\partial u}\bigg|_{u=1/a_{\mathbb{C}}}. \tag{4.22}$$

The term linear in u modifies the frequency of the orbit on the left-hand side of the equation of motion. The motion is now given by

$$\begin{aligned} u(\theta) &= u_{\mathbb{C}}(1 + \epsilon\cos\omega(\theta - \theta_0))(1 + \ldots), \\ \omega^2 &= 1 + \frac{u_{\mathbb{C}} a_{\mathbb{C}}^4}{G m_N^2}\partial_r^2 V_i(r)|_{r=a_{\mathbb{C}}}, \end{aligned} \tag{4.23}$$

where the ellipsis denotes irrelevant corrections to the overall magnitude of the orbit. Having $\omega \neq 1$ implies a precession of the perihelion, which can be seen using $\cos\omega(\theta - \theta_0) = \cos\omega(\theta - \theta_0 + \frac{2\pi n}{\omega})$. The precession angle between two rotations is finally given by

$$\delta\theta_i = -\pi\frac{a_{\mathbb{C}}^3}{G m_N^2(1 - \epsilon^2)}\partial_r^2 V_i(r)|_{r=a_{\mathbb{C}}}. \tag{4.24}$$

We apply this general formula to the Casimir-Polder potentials of Eq. (2.2). Interestingly, the V_a and V_c potentials, which are attractive, induce an advance of the perihelion while V_b, which is repulsive, induces a delay of the perihelion.

The Moon precession angle is constrained by lunar laser ranging experiments. Other well-understood perturbations induce Moon's orbit precession: the quadrupole field of the Earth, other bodies of the solar system, and general relativity. Once all these effects are taken into account, one obtains a bound on an extra, anomalous precession angle. Following Ref. [2], an experimental limit from lunar laser ranging is given as

$$\delta\theta_i < 2\pi \times 1.6 \times 10^{-11}. \tag{4.25}$$

V. BOUNDS ON FORCES FROM DARK SCALARS

Let us apply the experimental bounds obtained in Sec. IV to the Casimir-Polder forces from a dark scalar given in Eq. (2.2).

It is instructive first to understand qualitatively the landscape of exclusion regions on the Casimir-Polder forces. Let us consider the exclusion regions for the Yukawa force (see *e.g.,* [3]). Starting from large scales, the reach of the experiment starts to decrease very steeply below the scale of the Eöt-Wash experiment, at roughly $\lambda < O(10^{-4}\text{ m})$ down to atomic scales. In this region of λ, the bound on the strength of the Yukawa force α scales very roughly as $\alpha < 10^{-22}(\frac{1\text{m}}{\lambda})^5$, demonstrating the increasing difficulties in measuring forces at small distances. The Casimir-Polder forces behave as $1/r^n$ with $n \geq 3$ at short distance. This has the crucial implication that the constraints from short distance experiments will gain importance and those from long distance will lose importance compared to the exclusion regions on the Yukawa-like force. In particular, one can expect the Eöt-Wash bound to dominate over the bounds from all experiments at larger scale, to the possible exception of lunar laser ranging. Moreover, when $n = 7$, the decrease of sensitivity in λ^{-5} is expected to be overwhelmed by the increase of the force in r^{-7}, implying that bounds from the experiments at the smallest scales (from neutron scattering and molecular spectroscopy) dominate over all the bounds from higher distances.

The exclusion regions for the V_a, V_b, V_c Casimir-Polder potentials are respectively presented in Figs. 2, 3, 4. For the V_a potential, we obtain that the Eöt-Wash bound (deduced from [70], Sec. IX B) is the dominant one for $\lambda > 10^{-3}$ m. For both V_b and V_c potentials, we obtain indeed an inversion in the hierarchy of bounds. The two leading bounds turn out to be from the $dd\mu^+$ molecular ion and from the neutron scattering bound combining optical and total cross sections. This fact can be taken as an incentive to pursue and develop such small scale experiments. We remind that, as explained in Sec. IV B, for the V_b and V_c potential, the $dd\mu^+$ observable has some dependence in

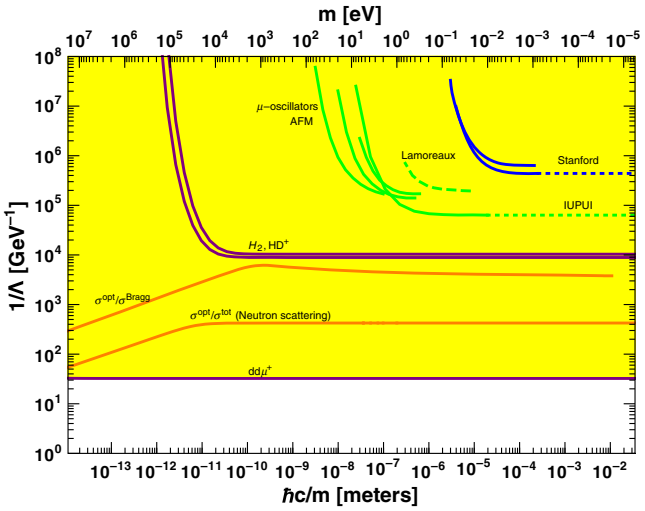

FIG. 4. Bounds on a scalar coupled to nucleons via the $\mathcal{O}_c$ interaction. Same conventions as Fig. 2.

$r_{\rm UV}$. In our computations, as is customarily done, $r_{\rm UV}$ is taken to be the radius of the deuteron.

Using the calculation given in 4.5, we obtain that limits from lunar laser ranging are indeed subleading. At zero mass, the bounds on Λ for the V_a, V_b, V_c potentials are found to be respectively $\Lambda > 2$ GeV, 6×10^{-5} eV, 2×10^{-8} eV. All these bounds are overwhelmed by stronger ones from shorter distance experiments.

VI. CONCLUSIONS

There are many motivations—including dark matter and dark energy—for speculating on the existence of a dark sector containing particles with a bilinear coupling to the Standard Model particles. Whenever one of the dark particles is light enough and couples to nucleons in a spin-independent way, it induces forces of the Casimir-Polder type, that are potentially accessible by fifth force experiments across many scales. The short- and long-range behaviors of these forces as well as their sign can all be understood and predicted using dimensional analysis and the optical theorem. We provide a comprehensive (re)interpretation of bounds from neutron scattering to the Moon perihelion precession, applicable to any kind of potential. We then focus on the case of a scalar with a variety of couplings to nucleons, generating forces with $1/r^3$, $1/r^5$, $1/r^7$ short-distance behaviors. It turns out that forces in $1/r^5$, $1/r^7$ are best constrained by neutron scattering and molecular spectroscopy, which provides extra motivation to pursue these kind of low-scale experiments. Implications for dark matter searches have been discussed in Ref. [6].

ACKNOWLEDGMENTS

This work is supported in part by the EU Horizon 2020 research and innovation program under the Marie-Sklodowska Grant No. 690575. S. F. thanks V. Korobov for important clarifications on molecular wave functions. This article is based upon work related to the COST Action CA15117 (CANTATA) supported by COST (European Cooperation in Science and Technology). S. F. was supported by the São Paulo Research Foundation (FAPESP) under Grants No. 2011/11973 and No. 2014/21477-2.

APPENDIX A: UV COMPLETIONS

In this Appendix, we consider models which lead to the operators $\mathcal{O}^0_{a,b,c}$ at low energy. We first show a simple model giving rise to $\mathcal{O}^0_b$, then we readily present a more general setting, which can be described in five dimensions using the AdS/CFT correspondence, and which can provide viable UV completions to any kind of dark particle and low-energy interaction we have considered in this paper and in [6].

1. Minimal scenario for $\mathcal{O}^0_b$: A light leptophobic Z'

For operator $\mathcal{O}^0_b$, let us assume that the quarks and ϕ are charged under an extra $U(1)$, whose gauge boson Z' has a mass $m_{Z'}$. Then, we have

$$\mathcal{L} \supset g_B Q_q Z_\mu J^\mu_q + g_B Q_\phi Z_\mu J^\mu_\phi. \tag{A1}$$

At low energy, the quarks go into nucleons, and the theory takes the form

$$\mathcal{L} \supset g_B Q_N Z_\mu J^\mu_N + g_B Q_\phi Z_\mu J^\mu_\phi. \tag{A2}$$

For $E < m_{Z'}$, one integrates out the Z' and the low-energy effective theory takes the form

$$\mathcal{L} \supset -\frac{1}{2m^2_{Z'}}(g_B Q_N J^\mu_N + g_B Q_\phi J^\mu_\phi)^2. \tag{A3}$$

This gives

$$1/\Lambda^2 = -g_B Q_N g_\phi Q_\phi m^{-2}_{Z'} \tag{A4}$$

and also a four-nucleon interaction that could be tested by neutron scattering.

A light-enough Z' is inaccessible at the LHC [71]. Other bounds have been discussed in [6,72–76]. The Z' is assumed to be leptophobic; hence, the theory has gauge anomalies, which should be canceled by new chiral fermions which cannot be arbitrarily heavy. Recent development on meson decays via Z' [77,78] seem also to put challenging bounds on Λ (see [77]), in which case the fifth force bounds would need to be improved by several order of magnitudes to be competitive on this minimal Z' scenario. However, this scenario can be embedded in the framework of next section, in which case experimental constraints from mesons, colliders are relaxed.

2. UV completion from a sub-GeV warped extra dimension

There is a scenario in which the dark particles automatically decouple from the SM sector above a scale which can be chosen arbitrarily low. This scenario is fully general in the sense that it applies to any kind of dark particle and of operators considered in this paper. This decoupling property was first noted in [15] in a different context. This automatic decoupling between the SM and the dark sector happens when the latter is a strongly interacting theory which is conformal in the UV and which develops bound states in the IR. Although the mechanism may apply in other cases, we focus here on large N_c and large t'Hooft coupling, in which case the AdS/CFT correspondence applies and quantitative features can thus be easily obtained.

The CFT bound states identified as the dark particles appear below a scale μ—which will typically be below $\Lambda_{\rm QCD}$ in our context. All the SM fields are assumed to be elementary, and the CFT bound states will form the dark sector. The key feature of this scenario is that above the scale of conformal breaking μ, the CFT bound states become invisible to elementary SM fields. This scenario has a number of attractive features which do not need to be discussed here. In this Appendix, we lay down only the aspects relevant in order to UV-complete the operators studied in this paper, and the five-dimensional computations are not detailed.

Let us use a five-dimensional model to illustrate concretely what happens. We consider a slice of AdS_5 with curvature $k \sim M_{\rm Pl}$ where the nucleons—and the other SM fields remaining below $\Lambda_{\rm QCD}$— are on the UV brane, at $z_0 = 1/k$. We assume that the ϕ field is purely composite and lies thus on the IR brane at $z_1 = 1/\mu$. The mediator X is a bulk field, chosen here to be a scalar Φ with Neumann boundary conditions, and which induces interactions between the fields of two branes i.e., between the SM and the dark sector.

The Lagrangian including brane interactions is

$$S = \int d^4x^\mu dz \sqrt{-g}\left(\frac{1}{2}\nabla_M\Phi\nabla^M\Phi - \frac{1}{2}m_\Phi^2\Phi^2 + \lambda\delta(z-z_0)\bar{N}N\Phi + \kappa\delta(z-z_1)\phi^2\Phi\right). \tag{A5}$$

The typical values of the parameters are $\lambda = 1/\sqrt{k}$, $\kappa = \mu/\sqrt{k}$ The bulk mass has to satisfy the Breitenlohner-Freedman bound, $m_\Phi^2 \geq -4k^2$ to prevent tachyonic instabilities in AdS_5.

For further convenience the bulk mass will be parametrized as $m_\Phi^2 = (-3-2\epsilon+\epsilon^2)k^2$. If the boundary conditions were tuned it could have a zero mode, but here such an assumption is unnecessary, our interest rather lies in the Kaluza-Klein modes. The KK mode wave functions have values on the UV brane which are the largest for $\epsilon = 0$, and decrease exponentially for $|\epsilon| > 0$. For concreteness we consider the case with a nonzero IR brane mass $\delta(z-z_1)b_{\rm IR}k\Phi^2/2$ and a zero UV brane mass.

To illustrate our point, we consider the $N\phi \to N\phi$ amplitude for $q > \mu$, where q is the center of mass energy of the process. For ϵ slightly larger than zero (so that $(\mu/k)^\epsilon \ll 1$), one finds

$$i\mathcal{M} \propto i\lambda\kappa\frac{\sqrt{\pi}}{\Gamma(\epsilon)}\frac{1}{\sqrt{k\mu}}\left(\frac{2k}{q}\right)^{3/2-\epsilon}e^{-\frac{q}{\mu}}. \tag{A6}$$

We see that an exponential suppression of the amplitude occurs. This shows how the CFT states become invisible to the elementary fields above μ.

Let us now consider $q \ll \mu$ and compute the nucleon-dark particle interaction induced by the KK modes, *i.e.,* by the CFT bound states in the dual picture. All the KK modes are integrated out, and for ϵ slightly larger than 0, we find the nucleon–dark particle interaction to be

$$\mathcal{L}_{\rm 4D} \supset -\left(\frac{1}{2}\lambda^2\frac{k(2+2\epsilon-b_{\rm IR})}{\mu^2 b_{\rm IR}(2+2\epsilon)k}\left(\frac{\mu}{k}\right)^{2\epsilon}(\bar{N}N)^2 + \lambda\kappa\frac{k}{b_{\rm IR}\mu^2}\left(\frac{\mu}{k}\right)^{\epsilon}\bar{N}N\phi^2 + \frac{1}{2}\kappa^2\frac{k}{b_{\rm IR}\mu^2}\phi^4\right) \tag{A7}$$

$$\sim -\left(\frac{1}{2\mu^2}\left(\frac{\mu}{k}\right)^{2\epsilon}(\bar{N}N)^2 + \frac{1}{\mu}\left(\frac{\mu}{k}\right)^{\epsilon}\bar{N}N\phi^2 + \frac{1}{2}\phi^4\right). \tag{A8}$$

where the $\mathcal{O}_a^0$ contact operator between SM and dark particle appears, with effective scale

$$\Lambda = \mu\left(\frac{k}{\mu}\right)^{\epsilon}. \tag{A9}$$

We can see a hierarchy between the contact interactions, simply because the mediators couple strongly to the DS and weakly to the SM. The SM self interaction is suppressed with respect to the SM-dark particle interaction, and the dark particle is strongly self-interacting.

A very similar analysis can be done for *any* kind of IR brane operator and bulk mediator. For example a derivative coupling of the form $\delta(z-z_1)\Phi(\partial^\mu\phi)^2$ would occur if ϕ is a Nambu-Goldstone boson. This generates the $\mathcal{O}_c^0$ operator. In our setup, there is no source of explicit breaking of the global symmetry; hence, the GB is massless. However, a mass term parametrizing a source of explicit symmetry breaking can always be introduced—in which case brane operators of the form $\delta(z-z_1)m^2\phi^2\Phi$ should also taken into account, which will contribute to $\mathcal{O}_a^0$. Finally, we note that the CFT sector can be approximately supersymmetric, as first noticed in [15], letting a scalar dark particle be arbitrarily lighter than μ. One can verify using [6] that there are no cancellations in the Casimir-Polder force in presence of superpartners.

APPENDIX B: CALCULATION OF THE POTENTIALS

This Appendix contains details of the computation for the potentials in Eq. (2.2) and those given in Ref. [6]. The full set of operators considered is

$$\mathcal{O}^0_a = \frac{1}{\Lambda}\bar{N}N|\phi|^2, \qquad \mathcal{O}^0_b = \frac{1}{\Lambda^2}\bar{N}\gamma^\mu N\phi^* i\overleftrightarrow{\partial}_\mu\phi,$$
$$\mathcal{O}^0_c = \frac{1}{\Lambda^3}\bar{N}N\partial^\mu\phi^*\partial_\mu\phi, \qquad \mathcal{O}^{1/2}_a = \frac{1}{\Lambda^2}\bar{N}N\bar{\chi}\chi,$$
$$\mathcal{O}^{1/2}_b = \frac{1}{\Lambda^2}\bar{N}\gamma^\mu N\bar{\chi}\gamma^\mu\chi, \qquad \mathcal{O}^{1/2}_c = \frac{1}{\Lambda^2}\bar{N}\gamma^\mu N\bar{\chi}\gamma^\mu\gamma^5\chi,$$
$$\mathcal{O}^1_a = \frac{1}{\Lambda^3}\bar{N}N|mX^\mu + \partial^\mu\pi|^2,$$
$$\mathcal{O}^1_b = \frac{1}{\Lambda^2}2\bar{N}\gamma^\mu N\mathrm{Im}(X_{\mu\nu}X^{\nu*} + \partial^\nu(X_\nu X^*_\mu) + \partial^\mu\bar{c}c^*),$$
$$\mathcal{O}^1_c = \frac{1}{\Lambda^3}\bar{N}N|X^{\mu\nu}|^2, \qquad \mathcal{O}^1_d = \frac{1}{\Lambda^3}\bar{N}NX^{\mu\nu}\tilde{X}^*_{\mu\nu}. \tag{B1}$$

A dark particle of spin 0, 1/2, 1 is denoted by ϕ, χ, X. π and c, $\bar{c}$ are respectively the Goldstone bosons and ghosts accompanying X. At that point the dark particle can be self-conjugate (real scalar or vector, Majorana fermion) or not (complex scalar or vector, Dirac fermion). When X is complex, so are π, c and $\bar{c}$. We will give the results for all cases. We introduce

$$\eta = \begin{cases} 0 & \text{if self-conjugate} \\ 1 & \text{otherwise.} \end{cases} \tag{B2}$$

We calculate the loop diagram of Fig. 1 induced by each of these operators using dimensional regularization. The matching of the effective theory with the UV theory being done at the scale Λ, we can readily identify the divergent integrals as (see [79,80])[6]

$$\int \frac{d^4l}{(2\pi)^4}\frac{1}{(l^2-\Delta)^2} \to \frac{-i}{(4\pi)^2}\log(\Delta/\Lambda^2), \tag{B3}$$

$$\int \frac{d^4l}{(2\pi)^4}\frac{l^2}{(l^2-\Delta)^2} \to \frac{-2i}{(4\pi)^2}\Delta\log(\Delta/\Lambda^2), \tag{B4}$$

$$\int \frac{d^4l}{(2\pi)^4}\frac{(l^2)^2}{(l^2-\Delta)^2} \to \frac{-3i}{(4\pi)^2}\Delta^2\log(\Delta/\Lambda^2). \tag{B5}$$

From these amplitudes, the discontinuities in the non-relativistic scattering potential $\tilde{V}$ are given by Eq. (2.4) and are found to be

$$[\tilde{V}^0_a] = 2^\eta\frac{[f_0]}{32\pi^2\Lambda^2}$$
$$[\tilde{V}^0_b] = \eta\frac{m^2[f_0]-\lambda^2[f_1]}{8\pi^2\Lambda^4}$$
$$[\tilde{V}^0_c] = 2^\eta\frac{(6m^4+m^2\lambda^2)[f_0]-(24m^2\lambda^2+\lambda^4)[f_1]+20\lambda^4[f_2]}{64\pi^2\Lambda^6}$$
$$[\tilde{V}^{1/2}_a] = 2^\eta\frac{3(\lambda^2[f_1]-m^2[f_0])}{8\pi^2\Lambda^4}$$
$$[\tilde{V}^{1/2}_b] = \eta\frac{-\lambda^2[f_1]}{2\pi^2\Lambda^4}$$
$$[\tilde{V}^{1/2}_c] = 2^\eta\frac{m^2[f_0]-\lambda^2[f_1]}{4\pi^2\Lambda^4}$$
$$[\tilde{V}^1_a] = 2^\eta\frac{(6m^4-m^2\lambda^2)[f_0]-(12m^2\lambda^2+\lambda^4)[f_1]+20\lambda^4[f_2]}{64\pi^2\Lambda^6}$$
$$[\tilde{V}^1_b] = \eta\frac{(8m^2+5\lambda^2)[f_0]-10\lambda^2[f_1]}{16\pi^2\Lambda^4}$$
$$[\tilde{V}^1_c] = 2^\eta\frac{(9m^4+3m^2\lambda^2)[f_0]-(36m^2\lambda^2+3\lambda^4)[f_1]+30\lambda^4[f_2]}{8\pi^2\Lambda^6}$$
$$[\tilde{V}^1_d] = 2^\eta\frac{3(\lambda^4[f_1]-\lambda^2m^2[f_0])}{8\pi^2\Lambda^6} \tag{B6}$$

where the discontinuities of $f_{0,1,2}$ are given in Eq. (2.3). These loop functions are explicitly given by

$$f_0(m^2,q^2,\Lambda) = 2L\left(\frac{4m^2}{q^2}\right) + \log\left(\frac{m^2}{\Lambda^2}\right) \tag{B7}$$

$$f_1(m^2,q^2,\Lambda) = \frac{2m^2+q^2}{3q^2}L\left(\frac{4m^2}{q^2}\right) + \frac{1}{18} + \frac{1}{6}\log\left(\frac{m^2}{\Lambda^2}\right) \tag{B8}$$

$$f_2(m^2,q^2,\Lambda) = \frac{6m^4+2m^2q^2+q^4}{15q^4}L\left(\frac{4m^2}{q^2}\right) + \frac{13}{900} + \frac{m^2}{30q^2} + \frac{1}{30}\log\left(\frac{m^2}{\Lambda^2}\right) \tag{B9}$$

with

$$L(x) = \begin{cases} \sqrt{x-1}\arctan\left(\frac{1}{\sqrt{x-1}}\right) - 1 & \text{if } x > 1 \\ \sqrt{1-x}\left(i\pi + \frac{1}{2}\log\left(\frac{1+\sqrt{1-x}}{1-\sqrt{1-x}}\right)\right) - 1 & \text{if } x < 1. \end{cases} \tag{B10}$$

The $[f_n]$ discontinuities can be obtained by noticing that $\ln\Delta = \ln(x-x_+)(x-x_-)$ where

$$x_\pm = \frac{1}{2} \pm \frac{\sqrt{q^2-4m^2}}{2q} \tag{B11}$$

[6]The running of the Wilson coefficients is taken into account at leading-log order with this method.

has a branch cut between x_- and x_+ and a discontinuity of $2\pi i$. This leads to

$$[f_n] = 2\pi i \int_{x_-}^{x_+} (x(1-x))^n dx \tag{B12}$$

Finally, the spatial potential is given by Eq. (2.6). The integrals over λ needed in the last step of the calculation are

$$\int_{2m}^{\infty} d\lambda \sqrt{\lambda^2 - 4m^2} e^{-\lambda r} = \frac{2m}{r} K_1(2mr) \tag{B13}$$

$$\int_{2m}^{\infty} d\lambda \lambda^2 \sqrt{\lambda^2 - 4m^2} e^{-\lambda r} = \frac{8m^3}{r} K_1(2mr) + \frac{12m^2}{r^2} K_2(2mr) \tag{B14}$$

$$\int_{2m}^{\infty} d\lambda \lambda^4 \sqrt{\lambda^2 - 4m^2} e^{-\lambda r} = \frac{32m^4}{r^2} K_2(2mr) + \left(\frac{120m^3}{r^3} + \frac{32m^5}{r}\right) K_3(2mr). \tag{B15}$$

APPENDIX C: AMPLITUDES

The one-loop amplitudes induced by the operators $\mathcal{O}_a$, $\mathcal{O}_b$, $\mathcal{O}_c$ are

$$i\mathcal{M}_a = \frac{1}{2\Lambda^2} \bar{u}(p_1) u(p_2) \bar{u}(p_1') u(p_2') \times \int \frac{d^4k}{(2\pi)^4} \frac{1}{(k^2 - m^2)((k+q)^2 - m^2)} \tag{C1}$$

$$i\mathcal{M}_b = \frac{1}{\Lambda^4} \bar{u}(p_1) \gamma^\mu u(p_2) \bar{u}(p_1') \gamma^\nu u(p_2') \times \int \frac{d^4k}{(2\pi)^4} \frac{(q+2k)^\mu (q+2k)^\nu}{(k^2 - m^2)((k+q)^2 - m^2)} \tag{C2}$$

$$i\mathcal{M}_c = \frac{1}{2\Lambda^6} \bar{u}(p_1) u(p_2) \bar{u}(p_1') u(p_2') \times \int \frac{d^4k}{(2\pi)^4} \frac{(q.(q+k))^2}{(k^2 - m^2)((k+q)^2 - m^2)} \tag{C3}$$

with $q = p_1 - p_2$. These integrals can be reduced to the basis shown in Eqs. (B3)–(B5) using textbook techniques (see [79], including Feynman trick).

APPENDIX D: WAVE FUNCTIONS

This section displays the wave functions of the molecular and nuclear systems (respectively Figs. 5–7) used in Secs. IV B and IV D.

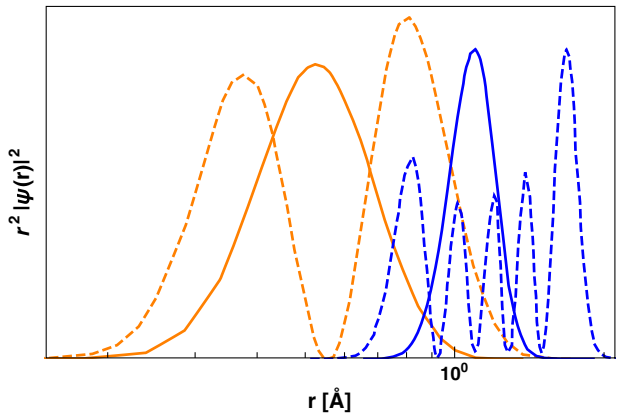

FIG. 5. Wave function densities of states considered for molecular spectroscopy in Sec. IV B. Orange: H_2, $(\nu = 0, J = 0)$ (plain) and $(\nu = 1, J = 0)$ (dashed) states. Blue: HD^+, $(\nu = 0, J = 2)$ (plain) and $(\nu = 4, J = 3)$ (dashed) states.

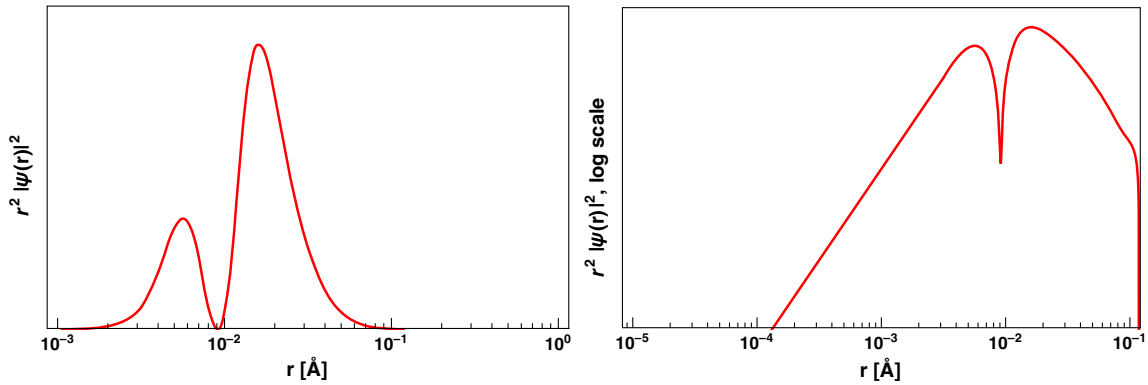

FIG. 6. Wave function density of the $(\nu = 1, J = 0)$ state of $dd\mu^+$ in linear scale (left) and log scale (right).

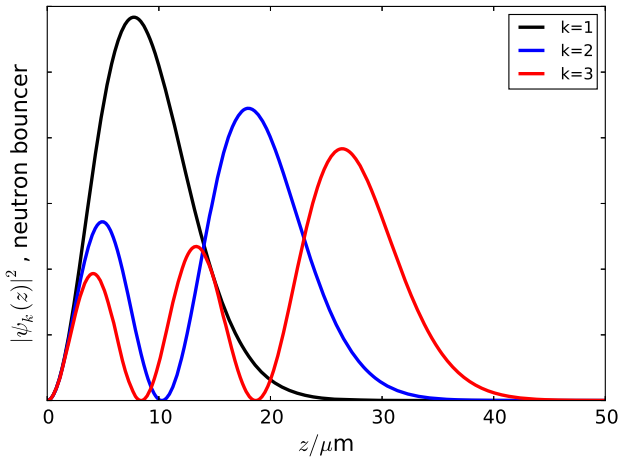

FIG. 7. Wave function densities of the three first quantum states of a bouncing neutron in a gravitational well.

[1] E. Fischbach and C. L. Talmadge, *The search for non-Newtonian gravity* (Springer, New York, 1999).

[2] E. G. Adelberger, B. R. Heckel, and A. E. Nelson, Tests of the gravitational inverse square law, Annu. Rev. Nucl. Part. Sci. **53**, 77 (2003).

[3] E. G. Adelberger, J. H. Gundlach, B. R. Heckel, S. Hoedl, and S. Schlamminger, Torsion balance experiments: A low-energy frontier of particle physics, Prog. Part. Nucl. Phys. **62**, 102 (2009).

[4] I. Antoniadis *et al.*, Short-range fundamental forces, C.R. Phys. **12**, 755 (2011).

[5] E. J. Salumbides, W. Ubachs, and V. I. Korobov, Bounds on fifth forces at the sub-Angstrom length scale, J. Mol. Spectrosc. **300**, 65 (2014).

[6] S. Fichet, Quantum Forces from Dark Matter and Where to Find Them, Phys. Rev. Lett. **120**, 131801 (2018).

[7] H. B. G. Casimir and D. Polder, The influence of retardation on the London-van der Waals forces, Phys. Rev. **73**, 360 (1948).

[8] G. Feinberg and J. Sucher, Long-range forces from neutrino-pair exchange, Phys. Rev. **166**, 1638 (1968).

[9] A. L. Erickcek, P. J. Steinhardt, D. McCammon, and P. C. McGuire, Constraints on the interactions between dark matter and baryons from the x-ray quantum calorimetry experiment, Phys. Rev. D **76**, 042007 (2007).

[10] M. S. Mahdawi and G. R. Farrar, Closing the window on ~GeV Dark Matter with moderate ($\sim\mu$b) interaction with nucleons, J. Cosmol. Astropart. Phys. 12 (2017) 004.

[11] M. S. Mahdawi and G. R. Farrar, Constraints on Dark Matter with a moderately large and velocity-dependent DM-nucleon cross-section, arXiv:1804.03073.

[12] S. Fichet, Shining light on polarizable dark particles, J. High Energy Phys. 04 (2017) 088.

[13] A. Voigt and S. Westhoff, Virtual signatures of dark sectors in Higgs couplings, J. High Energy Phys. 11 (2017) 009.

[14] E. J. Copeland, M. Sami, and S. Tsujikawa, Dynamics of dark energy, Int. J. Mod. Phys. D **15**, 1753 (2006).

[15] T. Gherghetta and A. Pomarol, The standard model partly supersymmetric, Phys. Rev. D **67**, 085018 (2003).
[16] P. Brax, S. Fichet, and F. Tanedo (to be published).
[17] N. Kaloper, Disformal inflation, Phys. Lett. B **583**, 1 (2004).
[18] P. Brax and C. Burrage, Constraining disformally coupled scalar fields, Phys. Rev. D **90**, 104009 (2014).
[19] J. A. Grifols, E. Masso, and R. Toldra, Majorana neutrinos and long range forces, Phys. Lett. B **389**, 563 (1996).
[20] A. V. Manohar, Effective field theories, Lect. Notes Phys. **479**, 311 (1997).
[21] V. V. Nesvizhevsky and K. V. Protasov, Constraints on nonNewtonian gravity from the experiment on neutron quantum states in the earth's gravitational field, Classical Quantum Gravity **21**, 4557 (2004).
[22] H. Leeb and J. Schmiedmayer, Constraint on Hypothetical Light Interacting Bosons from Low-Energy Neutron Experiments, Phys. Rev. Lett. **68**, 1472 (1992).
[23] A. Frank, P. van Isacker, and J. Gomez-Camacho, Probing additional dimensions in the universe with neutron experiments, Phys. Lett. B **582**, 15 (2004).
[24] P. J. S. Watson, A Limit on short-range modifications to gravity, arXiv:hep-ph/0406308.
[25] G. L. Greene and V. P. Gudkov, A neutron interferometric method to provide improved constraints on non-Newtonian gravity at the nanometer scale, Phys. Rev. C **75**, 015501 (2007).
[26] S. Baessler, V. V. Nesvizhevsky, K. V. Protasov, and A. Yu. Voronin, A New constraint for the coupling of axion-like particles to matter via ultra-cold neutron gravitational experiments, Phys. Rev. D **75**, 075006 (2007).
[27] V. V. Nesvizhevsky, G. Pignol, and K. V. Protasov, Neutron scattering and extra short range interactions, Phys. Rev. D **77**, 034020 (2008).
[28] Y. Kamiya, K. Itagami, M. Tani, G. N. Kim, and S. Komamiya, Constraints on New Gravitylike Forces in the Nanometer Range, Phys. Rev. Lett. **114**, 161101 (2015).
[29] L. Koester, H. Rauch, and E.Seymann, Neutron scattering lengths: A survey of experimental data and methods, At. Data Nucl. Data Tables **49**, 65 (1991).
[30] M. Niu, E. Salumbides, G. Dickenson, K. Eikema, and W. Ubachs, Precision spectroscopy of the rovibrational splittings in h2, {HD} and {D2}, J. Mol. Spectrosc. **300**, 44 (2014).
[31] J. Biesheuvel, J. P. Karr, L. Hilico, K. S. E. Eikema, W. Ubachs, and J. C. J. Koelemeij, Probing QED and fundamental constants through laser spectroscopy of vibrational transitions in HD+, Nat. Commun. **7**, 10385 (2016).
[32] J. Biesheuvel, J.-P. Karr, L. Hilico, K. S. E. Eikema, W. Ubachs, and J. C. J. Koelemeij, High-precision spectroscopy of the HD^+ molecule at the 1-p.p.b. level, Appl. Phys. B **123**, 23 (2017).
[33] D. V. Balin *et al.*, High precision study of muon catalyzed fusion in d2 and hd gas, Phys. Part. Nucl. **42**, 185 (2011).
[34] M. Hori, A. Soter, D. Barna, A. Dax, R. Hayano, S. Friedreich, B. Juhasz, T. Pask, E. Widmann, D. Horvath, L. Venturelli, and N. Zurlo, Two-photon laser spectroscopy of antiprotonic helium and the antiproton-to-electron mass ratio, Nature (London) **475**, 484 (2011).
[35] J. C. J. Koelemeij, B. Roth, A. Wicht, I. Ernsting, and S. Schiller, Vibrational Spectroscopy of hd^+ with 2-ppb Accuracy, Phys. Rev. Lett. **98**, 173002 (2007).
[36] U. Bressel, A. Borodin, J. Shen, M. Hansen, I. Ernsting, and S. Schiller, Manipulation of Individual Hyperfine States in Cold Trapped Molecular Ions and Application to hd^+ Frequency Metrology, Phys. Rev. Lett. **108**, 183003 (2012).
[37] J. Liu, E. J. Salumbides, U. Hollenstein, J. C. J. Koelemeij, K. S. E. Eikema, W. Ubachs, and F. Merkt, Determination of the ionization and dissociation energies of the hydrogen molecule, J. Chem. Phys. **130**, 174306 (2009).
[38] J.-P. Karr, $H2+$ and HD: Candidates for a molecular clock, J. Mol. Spectrosc. **300**, 37 (2014).
[39] S. Schiller, D. Bakalov, and V. I. Korobov, Simplest Molecules as Candidates for Precise Optical Clocks, Phys. Rev. Lett. **113**, 023004 (2014).
[40] V. I. Korobov, J. C. J. Koelemeij, L. Hilico, and J.-P. Karr, Theoretical Hyperfine Structure of the Molecular Hydrogen Ion at the 1 ppm Level, Phys. Rev. Lett. **116**, 053003 (2016).
[41] V. I. Korobov, L. Hilico, and J.-P. Karr, Theoretical transition frequencies beyond 0.1 ppb accuracy in H_2^+, HD^+, and antiprotonic helium, Phys. Rev. A **89**, 032511 (2014).
[42] K. Pachucki, Electrodynamics of a compound system with relativistic corrections, Phys. Rev. A **76**, 022106 (2007).
[43] K. Pachucki, Born-oppenheimer potential for h_2, Phys. Rev. A **82**, 032509 (2010).
[44] V. I. Korobov, Dynamic polarizability properties of the weakly bound $dd\mu$ and $dt\mu$ molecular ions, J. Phys. B **37**, 2331 (2004).
[45] V. I. Korobov, Leading-order relativistic and radiative corrections to the rovibrational spectrum of H_2^+ and Hd^+ molecular ions, Phys. Rev. A **74**, 052506 (2006).
[46] V. I. Korobov, Calculation of transitions between metastable states of antiprotonic helium including relativistic and radiative corrections of order $R_\infty\alpha^4$, Phys. Rev. A **77**, 042506 (2008).
[47] V. I. Korobov, Relativistic corrections of $m\alpha^6$ order to the rovibrational spectrum of H_2^+ and hd^+ molecular ions, Phys. Rev. A **77**, 022509 (2008).
[48] K. Piszczatowski, G. Łach, M. Przybytek, J. Komasa, K. Pachucki, and B. Jeziorski, Theoretical determination of the dissociation energy of molecular hydrogen, J. Chem. Theory Comput. **5**, 3039 (2009).
[49] J. Komasa, K. Piszczatowski, G. Łach, M. Przybytek, B. Jeziorski, and K. Pachucki, Quantum electrodynamics effects in rovibrational spectra of molecular hydrogen, J. Chem. Theory Comput. **7**, 3105 (2011).
[50] E. J. Salumbides, J. C. J. Koelemeij, J. Komasa, K. Pachucki, K. S. E. Eikema, and W. Ubachs, Bounds on fifth forces from precision measurements on molecules, Phys. Rev. D **87**, 112008 (2013).
[51] E. J. Salumbides, A. N. Schellekens, B. Gato-Rivera, and W. Ubachs, Constraints on extra dimensions from precision molecular spectroscopy, New J. Phys. **17**, 033015 (2015).
[52] W. Ubachs, J. Koelemeij, K. Eikema, and E. Salumbides, Physics beyond the standard model from hydrogen spectroscopy, J. Mol. Spectrosc. **320**, 1 (2016).
[53] V. Korobov (private communication).

[54] M. Bordag, *Advances in the Casimir Effect*, International Series of Monographs (Oxford University Press, New York, 2009).
[55] S. J. Smullin, A. A. Geraci, D. M. Weld, J. Chiaverini, S. P. Holmes, and A. Kapitulnik, New constraints on Yukawa-type deviations from Newtonian gravity at 20 microns, Phys. Rev. D **72**, 122001 (2005); Erratum, Phys. Rev. D **72**, 129901 (2005).
[56] Y. J. Chen, W. K. Tham, D. E. Krause, D. Lopez, E. Fischbach, and R. S. Decca, Stronger Limits on Hypothetical Yukawa Interactions in the 30–8000 nm Range, Phys. Rev. Lett. **116**, 221102 (2016).
[57] S. K. Lamoreaux, Demonstration of the Casimir Force in the 0.6 to 6 Micrometers Range, Phys. Rev. Lett. **78**, 5 (1997); Erratum, Phys. Rev. Lett. **81**, 5475 (1998).
[58] E. Fischbach, D. E. Krause, V. M. Mostepanenko, and M. Novello, New constraints on ultrashort ranged Yukawa interactions from atomic force microscopy, Phys. Rev. D **64**, 075010 (2001).
[59] R. S. Decca, D. Lopez, E. Fischbach, G. L. Klimchitskaya, D. E. Krause, and V. M. Mostepanenko, Tests of new physics from precise measurements of the Casimir pressure between two gold-coated plates, Phys. Rev. D **75**, 077101 (2007).
[60] R. S. Decca, D. Lopez, E. Fischbach, G. L. Klimchitskaya, D. E. Krause, and V. M. Mostepanenko, Novel constraints on light elementary particles and extra-dimensional physics from the Casimir effect, Eur. Phys. J. C **51**, 963 (2007).
[61] R. S. Decca, D. Lopez, H. B. Chan, E. Fischbach, D. E. Krause, and C. R. Jamell, Constraining New Forces in the Casimir Regime Using the Isoelectronic Technique, Phys. Rev. Lett. **94**, 240401 (2005).
[62] P. Brax, S. Fichet, and G. Pignol (to be published).
[63] V. V. Nesvizhevsky and K. V. Protasov, Constraints on nonNewtonian gravity from the experiment on neutron quantum states in the earth's gravitational field, Classical Quantum Gravity **21**, 4557 (2004).
[64] P. Brax and G. Pignol, Strongly Coupled Chameleons and the Neutronic Quantum Bouncer, Phys. Rev. Lett. **107**, 111301 (2011).
[65] P. Brax, G. Pignol, and D. Roulier, Probing strongly coupled chameleons with slow neutrons, Phys. Rev. D **88**, 083004 (2013).
[66] T. Jenke *et al.*, Gravity Resonance Spectroscopy Constrains Dark Energy and Dark Matter Scenarios, Phys. Rev. Lett. **112**, 151105 (2014).
[67] G. Pignol, Probing Dark Energy models with neutrons, Int. J. Mod. Phys. A **30**, 1530048 (2015).
[68] G. Cronenberg, H. Filter, M. Thalhammer, T. Jenke, H. Abele, and P. Geltenbort, A Gravity of Earth Measurement with a qBOUNCE Experiment, in *Proceedings, 2015 European Physical Society Conference on High Energy Physics (EPS-HEP 2015): Vienna, Austria, 2015* [*Proc. Sci.* EPS-HEP2015, 408 (2015)].
[69] J. G. Williams, S. G. Turyshev, and D. H. Boggs, Progress in Lunar Laser Ranging Tests of Relativistic Gravity, Phys. Rev. Lett. **93**, 261101 (2004).
[70] C. D. Hoyle, D. J. Kapner, B. R. Heckel, E. G. Adelberger, J. H. Gundlach, U. Schmidt, and H. E. Swanson, Sub-millimeter tests of the gravitational inverse-square law, Phys. Rev. D **70**, 042004 (2004).
[71] V. Khachatryan *et al.* (CMS Collaboration), Search for dark matter, extra dimensions, and unparticles in monojet events in proton–proton collisions at $\sqrt{s} = 8$ TeV, Eur. Phys. J. C **75**, 235 (2015).
[72] B. Batell, P. deNiverville, D. McKeen, M. Pospelov, and A. Ritz, Leptophobic dark matter at neutrino factories, Phys. Rev. D **90**, 115014 (2014).
[73] M. Ablikim *et al.* (BES Collaboration), Search for the Invisible Decay of J/psi in psi(2S)—pi+ pi− J/psi, Phys. Rev. Lett. **100**, 192001 (2008).
[74] B. A. Dobrescu and C. Frugiuele, GeV-Scale Dark Matter: Production at the main injector, J. High Energy Phys. 02 (2015) 019.
[75] N. Fernandez, J. Kumar, I. Seong, and P. Stengel, Complementary constraints on light dark matter from heavy quarkonium decays, Phys. Rev. D **90**, 015029 (2014).
[76] C. Frugiuele, Probing sub-GeV dark sectors via high energy proton beams at LBNF/DUNE and MiniBooNE, Phys. Rev. D **96**, 015029 (2017).
[77] J. A. Dror, R. Lasenby, and M. Pospelov, Dark forces coupled to nonconserved currents, Phys. Rev. D **96**, 075036 (2017).
[78] P. Ilten, Y. Soreq, M. Williams, and W. Xue, Serendipity in dark photon searches, arXiv:1801.04847.
[79] M. Peskin and D. Schroeder, *An Introduction to Quantum Field Theory* Advanced book classics. (Addison-Wesley, Reading, MA, 1995).
[80] S. Alam, S. Dawson, and R. Szalapski, Low-energy constraints on new physics revisited, Phys. Rev. D **57**, 1577 (1998).